The Journal of Chemical Physics

Temperature dependence of the photodissociation of CO_2 from high vibrational levels: 205-230 nm imaging studies of $CO(X^1\Sigma^+)$ and $O(^3P, ^1D)$ products

Cite as: J. Chem. Phys. **147**, 013916 (2017); https://doi.org/10.1063/1.4979952
Submitted: 25 January 2017 • Accepted: 28 March 2017 • Published Online: 20 April 2017

S. Sutradhar, B. R. Samanta, A. K. Samanta, et al.

Temperature dependence of the photodissociation of CO_2 from high vibrational levels: 205-230 nm imaging studies of $CO(X^1\Sigma^+)$ and $O(^3P, ^1D)$ products

S. Sutradhar, B. R. Samanta, A. K. Samanta,[a] and H. Reisler[b]
Department of Chemistry, University of Southern California, Los Angeles, California 90089-0482, USA

(Received 25 January 2017; accepted 28 March 2017; published online 20 April 2017)

The 205-230 nm photodissociation of vibrationally excited CO_2 at temperatures up to 1800 K was studied using Resonance Enhanced Multiphoton Ionization (REMPI) and time-sliced Velocity Map Imaging (VMI). CO_2 molecules seeded in He were heated in an SiC tube attached to a pulsed valve and supersonically expanded to create a molecular beam of rotationally cooled but vibrationally hot CO_2. Photodissociation was observed from vibrationally excited CO_2 with internal energies up to about 20 000 cm^{-1}, and $CO(X^1\Sigma^+)$, $O(^3P)$, and $O(^1D)$ products were detected by REMPI. The large enhancement in the absorption cross section with increasing CO_2 vibrational excitation made this investigation feasible. The internal energies of heated CO_2 molecules that absorbed 230 nm radiation were estimated from the kinetic energy release (KER) distributions of $CO(X^1\Sigma^+)$ products in $v'' = 0$. At 230 nm, CO_2 needs to have at least 4000 cm^{-1} of rovibrational energy to absorb the UV radiation and produce $CO(X^1\Sigma^+) + O(^3P)$. CO_2 internal energies in excess of 16 000 cm^{-1} were confirmed by observing $O(^1D)$ products. It is likely that initial absorption from levels with high bending excitation accesses both the A^1B_2 and B^1A_2 states, explaining the nearly isotropic angular distributions of the products. $CO(X^1\Sigma^+)$ product internal energies were estimated from REMPI spectroscopy, and the KER distributions of the $CO(X^1\Sigma^+)$, $O(^3P)$, and $O(^1D)$ products were obtained by VMI. The CO product internal energy distributions change with increasing CO_2 temperature, suggesting that more than one dynamical pathway is involved when the internal energy of CO_2 (and the corresponding available energy) increases. The KER distributions of $O(^1D)$ and $O(^3P)$ show broad internal energy distributions in the $CO(X^1\Sigma^+)$ cofragment, extending up to the maximum allowed by energy but peaking at low KER values. Although not all the observations can be explained at this time, with the aid of available theoretical studies of CO_2 VUV photodissociation and O + CO recombination, it is proposed that following UV absorption, the two lowest lying triplet states, a^3B_2 and b^3A_2, and the ground electronic state are involved in the dynamical pathways that lead to product formation. *Published by AIP Publishing.* [http://dx.doi.org/10.1063/1.4979952]

I. INTRODUCTION

Carbon dioxide is one of the most important molecules in the solar system. On Earth it is a known product of combustion and flames.[1–3] In space it is a ubiquitous component of ices in the interstellar medium and constitutes a major part of the atmospheres of Venus and Mars.[4–7] Not surprising, its behavior has been examined at temperatures ranging from near zero to thousands of Kelvin. Its photoinitiated reactions have attracted much attention as well. CO_2 possesses several close-lying excited singlet and triplet states whose interactions are not yet fully understood. Because the ground state of CO_2 is linear and the lowest excited electronic states are bent (~120°),[8–11] Franck-Condon (FC) factors connecting the ground vibrational levels of the ground and lowest excited states are vanishingly small.

In contrast to the many studies of the VUV photodissociation of CO_2,[12–27] where absorption cross sections from the ground vibrational state are large, very little is known about the photodissociation at energies closer to the lowest dissociation threshold to $O(^3P) + CO(X^1\Sigma^+)$, which is just above the band origins of the lowest excited singlet states, A^1B_2 and B^1A_2.[9,10] This dissociation channel is spin forbidden and can be reached only via spin-orbit coupling. In fact, theory reveals that five states (3 singlets and 2 triplets) may be involved in the evolution from the optically excited singlet state to the lowest dissociation channel. These states are connected by conical intersections and spin-orbit couplings at various internuclear distances and bond angles on the potential energy surfaces (PESs). Consequently, the couplings to the dissociation continuum are likely to involve multiple PESs.[8–11] The aforementioned photodissociation dynamics is found in several other isoelectronic 16-electron molecules, such as N_2O, OCS, and HNCO, all of which exhibit linear to strongly bent electronic transitions.[28]

For example, previous work on HNCO identified several dissociation pathways following initial photoexcitation to the bent S_1 state and terminating in $NH(X^3\Sigma^-) + CO(X^1\Sigma^+)$: $S_1 \rightarrow T_1 \rightarrow$ products; $S_1 \rightarrow S_0 \rightarrow T_1 \rightarrow$ products; and $S_1 \rightarrow T_2 \rightarrow T_1 \rightarrow$ products.[29–33] These pathways persist at high

[a]Current address: Center for Free-Electron Laser Science, DESY, Notkestrasse 85, 22607 Hamburg, Germany.
[b]Email: reisler@usc.edu

excitation energies, even when the allowed singlet product channels are open. In addition, Crim and coworkers carried out vibrationally mediated photodissociation experiments on HNCO, demonstrating vibrational state-specific effects on surface crossings.[34,35]

While ground state CO_2 does not absorb at wavelengths longer than 190 nm,[36,37] highly vibrationally excited CO_2 can absorb radiation even at 300 nm.[38–41] As a result, its photodissociation can be studied at much lower energies — closer to the lowest dissociation threshold. A large red shift in CO_2 absorption has been observed at high temperatures,[38–41] and several investigators estimated the average internal energy that CO_2 must possess in order to absorb at specific wavelengths. At 230 nm, for example, this was estimated at 0.5–1.2 eV.[40,42,43] While O and CO fragments have been detected before, the influence of "hot band" absorptions on the photodissociation dynamics has not been explored.

As stated above, theoretical calculations identify multiple surface crossings leading to dissociation. Several theoretical papers report CO_2 absorption cross sections and identify state interactions among the five lowest singlet and triplet states.[8–11] Bending and asymmetric stretch modes are identified as tuning and promoting modes, respectively, in the conical intersections among singlet states. Several theoretical studies address the recombination of $O(^3P)$ and CO to the ground singlet state of CO_2, which must involve spin-orbit couplings.[42,44–48]

The interest in the behavior of CO_2 in high temperature environments has also prompted extensive studies of its rovibrational spectroscopy. The well-known Fermi resonance between the CO_2 symmetric stretch and two quanta of bend leads to a complicated vibrational band structure,[49] with vibrational transitions organized in polyads. Vibrational spectra and cross sections have been published for levels up to $\sim$10 000 cm^{-1}.[50–56]

Here we report a Velocity Map Imaging (VMI) study of the effects of vibrational temperature on the photodissociation dynamics of CO_2 at 205–230 nm. Heating CO_2 up to $\sim$1800 K is achieved in an SiC tube attached to a pulsed valve, and the supersonically expanded hot molecules are then photodissociated by pulsed laser irradiation. Whereas the rotational temperature is reduced in the supersonic expansion to 50–150 K,[57,58] vibrational levels are cooled much less effectively. CO_2 molecules that remain in high vibrational levels absorb the radiation and dissociate. Depending on the CO_2 temperature, we observe one or both of the following channels (D_0 denotes the bond dissociation energy for each channel):[24]

$$CO_2 \rightarrow CO(X^1\Sigma^+) + O(^3P) \qquad D_0 = 43\,954\ cm^{-1}, \qquad \text{(I)}$$

$$CO_2 \rightarrow CO(X^1\Sigma^+) + O(^1D) \qquad D_0 = 59\,847\ cm^{-1}. \qquad \text{(II)}$$

We show that the kinetic energy release (KER) distributions obtained when monitoring $CO(X^1\Sigma^+)$ products in $v'' = 0$ provide information on the initial internal energy of the parent CO_2. The extent of internal excitation in the CO product is revealed from the images of $O(^3P)$ and $O(^1D)$ products. Photodissociation is observed only when the minimum vibrational excitation in CO_2 required for absorption at each excitation wavelength is reached.

II. EXPERIMENTAL DETAILS

Vibrationally excited CO_2 molecules are generated by passing a mixture of CO_2 (1%–5%) seeded in helium at a total pressure of 1.7 atm through a piezoelectrically driven pulsed valve operating at 10 Hz onto a resistively heated SiC tube (3.7 cm long, 1 mm id). The SiC tube is attached to two copper electrodes, which resistively heat an $\sim$1.5 cm long section of the tube.[59] The temperature of the SiC tube is estimated by the color of its glow.[60] Assuming that the hot SiC tube is a blackbody radiator, red, orange, and yellow colors are correlated (according to the International Commission on Illumination (CIE) chromaticity diagram[61]) with temperatures of 800–1000, 1200–1400, and 1600–1800 K, respectively. The corresponding temperatures are referred to in this work as low (red), medium (orange), and high (yellow). Each temperature range corresponds to a specific value of current in our heating arrangement and, as discussed below, leads to reproducible KER distributions of the CO and O products, thereby providing reliable trends as a function of CO_2 internal excitation.

The heated gas mixture is supersonically expanded into the source region of the vacuum chamber and passes through a skimmer (Beam Dynamics, 1.0 mm orifice diameter) to form a molecular beam that reaches the interaction region. As a result, the amount of internal energy of CO_2 in the molecular beam depends both on the extent of heating in the SiC tube and the subsequent cooling by supersonic expansion. A detailed description of the gas dynamics in a pyrolysis nozzle and the properties of the subsequent supersonic expansion is given by Ellison and coworkers.[57,58,62] The rotational temperature is estimated from Resonance Enhanced Multiphoton Ionization (REMPI) spectra of CO molecules under the same expansion conditions, and it increases from 50 K to 150 K as the temperature is increased up to 1800 K, in agreement with previous results.[57,58] The extent of vibrational excitation is discussed in Section III.

The molecular beam is intersected at a right angle by the laser beam at the center of the interaction region, where internally excited CO_2 molecules absorb UV radiation. Pulsed radiation at 225–230 nm (0.5 mJ/pulse, focused by a 30 cm f.l. lens) is generated by the frequency doubled output of a dye laser (Continuum ND6000, Coumarin dyes) pumped by the third harmonic output of a pulsed Nd:YAG laser (Continuum, PL8000). Laser radiation at 205.47 nm (0.1–0.2 mJ/pulse, focused by a 30 cm f.l. lens) is generated by mixing the fundamental (616.42 nm) of a dye laser (Continuum ND6000, DCM dye) and its frequency doubled output (308.21 nm).

$CO(X^1\Sigma^+, v'' = 0, 1, 2)$ products are ionized by 2+1 Resonance Enhanced Multiphoton Ionization (REMPI) at 230.1–230.5 nm via the $B^1\Sigma^+ \leftarrow X^1\Sigma^+$ transition.[63] $O(^3P_j)$ products are ionized by 2+1 REMPI at 225.6–226.4 nm via the $3p\ ^3P_{J'} \leftarrow 2p\ ^3P_{J''}$ transition,[64] and $O(^1D)$ products are ionized at 205.47 nm via the $3p\ ^1P_1 \leftarrow 2p\ ^1D_2$ transition.[65] Excitation of CO_2 and product detection are achieved at the same wavelength (one color experiment). Vibrationally excited CO_2 is detected by using 3+1 REMPI via the $3p\sigma_u\ ^1\Pi_u \leftarrow X^1\Sigma^+_g$ transition at 326–329 nm (2 mJ/pulse, focused by a 30 cm f.l. lens) generated from the frequency doubled output of a dye laser (Continuum ND6000, DCM/LDS 698) pumped by

the second harmonic output of a pulsed Nd:YAG laser.[66] The dependencies of the CO and O REMPI signals on laser fluence were investigated in order to assess possible contributions from multiphoton dissociation. The CO and O signals appear only with heated CO_2, and they persist even with laser energies as low as 0.2–0.3 mJ/pulse. Also, the KER distributions can only be explained consistently by assuming one-photon dissociation. We thus believe that multiphoton dissociation does not contribute significantly to the observed REMPI signals.

The experimental design and operation characteristics of our time-sliced velocity map imaging (VMI) arrangement have been described in detail before.[67–69] The ionized products are accelerated through a series of ion optics lenses in the flight tube toward a position sensitive detector (a phosphor screen coupled to a double-stack (40 mm dia) microchannel plates; Galileo Electro-Optics 3040FM series). A digital video-camera (PixeLINK PL-B741F) located behind the phosphor screen of the detector captures ion hit events produced by each laser firing, and the signal is transferred to a computer for further analysis. Sliced images of the ion cloud are obtained by fast gating of the detector (back plate of the MCP) using a home-built high-voltage pulser (5 ns fwhm, 2 kV peak).[68]

III. RESULTS AND DISCUSSION

A. REMPI spectra of CO products

CO products from photodissociation of hot CO_2 at ~230 nm under different heating conditions have been detected by 2+1 REMPI at the same wavelength. Figure 1 shows REMPI spectra obtained when the laser frequency is scanned in the region of the 2-photon $B^1\Sigma^+ - X^1\Sigma^+$ transition of CO.

The bandheads of the 0–0 (86 916 cm^{-1}) and 1–1 (86 856 cm^{-1}) vibronic peaks are assigned based on previous spectroscopic and photodissociation studies.[70,71] The CO photofragments have significant rotational excitation in both $v'' = 0$ and 1. Taking into account the calculated relative FC factors for the 0–0 and 1–1 transitions (1.00 and 0.91, respectively), we conclude that the relative population of $v'' = 1$ is low at all temperatures. Fit spectra of the 0–0 band, obtained using PGOPHER,[72] show that signal intensities drop significantly starting at $J'' > 14$, and signals are observed up to at least $J'' = 23$–24 with low heating. Rotational excitation in the 0–0 band increases with increased heating, and the distributions become clearly bimodal, displaying a weaker additional feature peaking at $J'' = 43$–44 and extending to at least $J'' > 47$. With increased heating, the second feature becomes more prominent. The total signal intensity increases strongly with increased heating.

To fit the rotational distribution of the 0–0 band, we used the expression

$$I(E) = A \sum_J (2J + 1) \cdot \Gamma(E - E_J) \cdot F(E_J), \quad (1)$$

where I is the observed line intensity at the 2-photon energy E, A is a scaling constant, $\Gamma(E - E_J)$ is the linewidth function (assumed Gaussian) for each rotational transition Q_{JJ} with energy E_J, and $F(E_J)$ is a fitting function. The Hönl-London factors for the Q-branch have been assumed to be constant.[73] In the above simulation, F is assumed to be a sum of two functions: a Boltzmann function $B(E_J, T)$ and a Gaussian distribution $G(E_{J^0} - E_J)$ centered at a specific rotational level J^0. The FWHM of the two Gaussian functions Γ and G, the rotational temperature T, and scaling constant A are varied to match the experimental distributions. An example is shown in Fig. 2 for the distribution obtained with high CO_2 heating.

The fits confirm that the observed bimodal rotational distributions for the 0–0 band consist of a statistical-like (Boltzmann) component and a Gaussian-shaped rotational component; their relative contributions vary with heating of the CO_2 parent molecule. Rotational excitation in $v'' = 1$ rises up to $J'' = 17$–18 at low temperatures and extends up to $J'' = 24$–25 with increased heating. We could not fit the 1–1 REMPI spectrum because of its partial overlap with the band starting at 86 800 cm^{-1}.

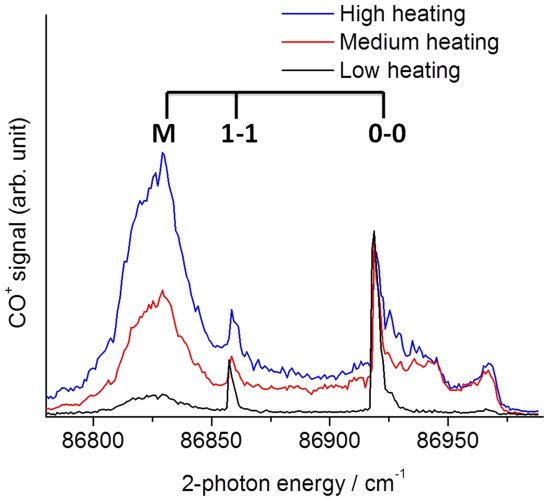

FIG. 1. One color 2+1 REMPI spectra of CO produced in the photodissociation of CO_2 around 230 nm recorded with low (black), medium (red), and high (blue) heating of the CO_2 parent, respectively. The REMPI transition from ground state vibrational level ($X^1\Sigma^+$, v'') to excited state vibrational level ($B^1\Sigma^+$, v') is denoted by v''-v'. The assignment of the band denoted by M is uncertain (see the text for discussion). Intensities are normalized to the 0–0 bandhead.

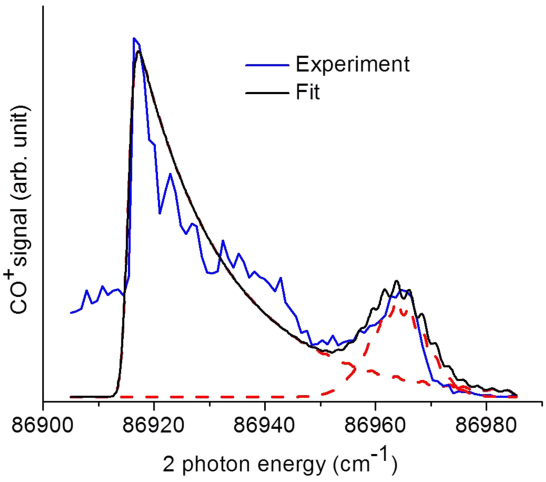

FIG. 2. Comparison of the REMPI spectrum of the CO 0–0 Q_{1J} band (blue) to a fit obtained with a rotational linewidth $\Gamma = 1.9\ cm^{-1}$, assuming a rotational temperature of 1700 K, and a Gaussian component with a width of 5 J'' levels centered at $J'' = 43$. The individual Boltzmann and Gaussian components are shown in red dashed lines and the total fit is shown in black.

The origin of the broad spectral feature with a maximum at ~86 830 cm^{-1} (denoted henceforth by M) is puzzling. This feature appears only at mass 28 in the time-of-flight mass spectrum, and only when irradiating hot CO_2. A similar feature has been observed by Spiglanin *et al.* in the REMPI spectrum of the CO product from the 193 nm photodissociation of HNCO[74] and tentatively assigned as the 2–2 vibronic band of this transition. However, we could not reproduce this feature using the known spectroscopic constants of the $B \leftarrow X$ transition. Even though the $B(v' = 0–9) - X(v'' = 0)$ vibronic bands of CO were investigated before,[63,70,75–78] due to crossings with repulsive states, the B state is severely predissociated at $v' > 1$.[70,75,79,80] As a result, the assignments of the band origins of the $B \leftarrow X$ vibronic transitions involving $v' > 1$ are quite uncertain, having large error bars. Using the known spectroscopic constants of the ground state,[81] and the experimental values for the v' levels in the B state, we have estimated the band origin frequencies of the diagonal transitions from 2–2 to 9–9 (see Table S1 in the supplementary material).

Boltzmann rotational distributions of the 2–2 and 5–5 vibronic transitions, whose spectral origins are closest to the M band, were simulated using PGOPHER.[72] Representative simulations are shown in Figs. S1 and S2 in the supplementary material. It is evident that the M band does not match well with any of the estimated $B \leftarrow X$ diagonal vibronic transitions. It is possible that this feature originates in a different electronic transition than $B \leftarrow X$. The three electronic states closest to this energy region are $k^3\Pi$, $C^1\Sigma_g^+$, and $E^1\Pi$.[82–84] The different vibronic transitions estimated from the known spectroscopic constants of these states are listed in Tables S2–S6 in the supplementary material. The only transition close to the M band is k $(v' = 1) \leftarrow X$ $(v'' = 2)$. The 500 K thermal rotational distribution of this vibronic transition is simulated (using PGOPHER) and is shown in Fig. S3 in the supplementary material. The simulated REMPI spectrum spans frequencies extending from near the bandhead of the 0–0 peak of the $B \leftarrow X$ transition to the low frequency end of the observed M band. The peak of the M band corresponds to $J'' = 5–10$ of $v'' = 2$ of the ground state. This transition may contribute to the REMPI signal originating in $v'' = 2$ of CO (see also Section III B), but other (yet unknown) transitions may contribute as well.

B. Kinetic energy release distributions of CO products

In order to obtain pair-correlated distributions, time-sliced images of $CO(X^1\Sigma^+, v'' = 0)$ were recorded at 230.1 nm (43 480 cm^{-1}) with different CO_2 heating levels, and the corresponding center of mass (c.m.) KER distributions are shown in Fig. 3.

Although the excitation energy (43 480 cm^{-1}) is slightly below the energy threshold of channel (I) (43 954 cm^{-1}), heating in the SiC tube imparts significant vibrational excitation to CO_2, and much of this excitation survives during supersonic expansion. Recall that only vibrationally hot CO_2 molecules can absorb at 230.1 nm. Since the $O(^3P)$ cofragments do not possess internal energy (except in their $^3P_1$ and $^3P_0$ spin-orbit states), the c.m. KER distributions obtained by monitoring the 0–0 bandhead, which is centered at low J'' levels, reflect the distribution of available energies in the dissociation and, therefore, also the initial rovibrational excitation of the heated parent CO_2 molecules.

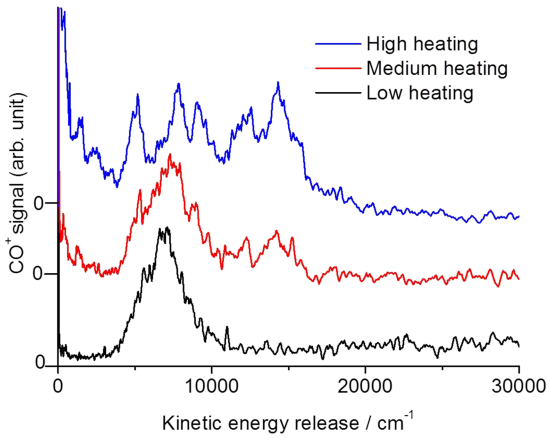

FIG. 3. Center-of-mass (c.m.) KER distributions obtained by monitoring $CO(X^1\Sigma^+, v'' = 0)$ products at 230.1 nm by 2+1 REMPI at the bandhead of the $B \leftarrow X$ (0–0) transition. Results are shown for low (black), medium (red), and high (blue) CO_2 heating. The relative signal intensities in the three plots are arbitrary.

It is evident from the KER distribution obtained with the lowest heating that the observed KER signal starts only at ~4000 cm^{-1}, corresponding to the minimum internal excitation that CO_2 must possess in order to absorb at 230.1 nm. This KER distribution extends up to about 10 000 cm^{-1}. With higher CO_2 heating, the vibrational excitation in the parent CO_2 molecules increases and reaches a maximum value of 17 000 –18 000 cm^{-1}, as shown in the middle and upper traces of Fig. 3. By energy conservation, KER values ranging between 4000 and ~16 000 cm^{-1} must be correlated only with the CO + $O(^3P)$ channel (channel (I)).

Referring to Fig. 3, the KER signal drops when the CO_2 internal excitation exceeds 17 000–18 000 cm^{-1} even with high level of heating. At the same time, an additional feature appears at low KER (0–2000 cm^{-1}). This feature corresponds to the opening of the CO + $O(^1D)$ channel (channel (II)), which lies 59 847 cm^{-1} above the ground state CO_2, or ~16 000 cm^{-1} above the CO + $O(^3P)$ channel threshold. In other words, channel (II) becomes energetically accessible at 230.1 nm when the available energy exceeds ~16 000 cm^{-1}.

It should be noted that the observed CO^+ signal intensities reflect two opposing factors: (1) the thermal population in the excited vibrational levels of CO_2, which decreases approximately exponentially with increasing vibrational energy, and (2) the absorption cross section at a specific temperature, which increases approximately exponentially with CO_2 internal energy at the long wavelength tail of the absorption curve.[1,6,38,40] Although the population of high vibrational levels is very small even with high heating (only 15% of the population exists in the energy region 4000–20 000 cm^{-1} at a temperature of 1800 K, assuming a Boltzmann distribution), the increased absorption cross sections make these levels visible in our experiments. As mentioned above, the final CO_2 internal energy distributions are determined by the extent of heating in the SiC tube and the subsequent cooling in the expansion, which evidently preserves much of the vibrational excitation. The structure in the KER distribution, which is most pronounced at higher temperatures, reflects the well-known clumpy nature of the CO_2 vibrational states,

which is also manifest in the polyad structure of its vibrational spectrum.[55]

We have also recorded time-sliced images of CO v″ = 1 by monitoring the bandhead of the $B \leftarrow X$ (1–1) transition at 230.27 nm, and the KER distribution is shown in Fig. 4(a).

The KER distribution corresponding to CO($X^1\Sigma^+$,v″ = 1) shows a sharp feature centered at 5000 cm^{-1} with a FWHM of ~1000 cm^{-1} and a low intensity broad feature extending up to about 18 000 cm^{-1}. However, analysis of the KER distribution of CO($X^1\Sigma^+$,v″ = 1) is complicated due to spectral overlap of the 1–1 bandhead with the M band. In order to separate the contribution of the M band to the 1–1 bandhead signal, the KER distribution in the M band region was obtained by recording sliced images at 230.34 nm (86 830 cm^{-1}) with different heating levels. An example, obtained with high heating, is displayed in Fig. 4(b), which shows that the narrow peak centered around 5000 cm^{-1} in the KER distribution is associated with the M band.

Since both KER distributions shown in Fig. 4 exhibit the same sharp feature centered at 5000 cm^{-1}, it is likely that this feature in the plot of CO v″ = 1 belongs to the underlying background of the M band. Indeed, the intensity of the sharp feature in Fig. 4(a) increases with increased heating as does the intensity of M band. In contrast, the broad features at higher KER values (Fig. 4(a)) do not increase appreciably with heating, in accordance with the behavior observed in the CO REMPI spectrum (Fig. 1). The background of the M band extends up to the bandhead of the 0–0 transition, where the images shown in Fig. 3 were recorded. With low heating, where the intensity of the M band is much smaller compared to the 0–0 bandhead, there is almost no feature at 5000 cm^{-1} in the KER distributions shown in Fig. 3. With increased heating, the KER distributions show the emergence of the 5000 cm^{-1} feature as the contribution from the M band increases. However, the M band contribution does not extend to higher rotational levels of the 0–0 band, and the KER distributions obtained by monitoring higher rotational levels ($J'' \geq 43$) of the 0–0 band do not show the 5000 cm^{-1} feature even with high heating (see Fig. S4 in the supplementary material). Evidently, a different dissociation mechanism, presently unknown, gives rise to the feature centered at ~5000 cm^{-1}.

C. Kinetic energy distributions of O(^{3}P, ^{1}D) products

Due to the uncertainty in the spectral assignment of the M band in the REMPI spectrum, it is best to assess the extent of CO internal excitation from the KER distributions of the atomic O(^{3}P$_j$) and O(^{1}D$_2$) photofragments. O(^{3}P$_j$) fragments (channel (I)) are detected by 2+1 REMPI at 225.6–226.6 nm, and the three spin orbit states (^{3}P$_2$, ^{3}P$_1$, and ^{3}P$_0$) produced in the photodissociation are shown in Fig. S5 in the supplementary material. The KER distributions obtained by monitoring O(^{3}P$_2$) with different heating levels of CO_2 are displayed in Fig. 5.

With low heating, the KER distribution exhibits a single broad feature extending from 0 to 10 000 cm^{-1}. An additional feature at 12 000–16 000 cm^{-1} appears with increased heating, indicating that two different dynamical pathways lead to channel (I). Similar results (not shown) are obtained when monitoring O(^{3}P$_1$) and O(^{3}P$_0$). We emphasize that the KER distributions include contributions from CO(v,J) cofragments generated by photolysis of all CO_2 molecules whose internal energies exceed ~4000 cm^{-1}. They indicate that the dissociating CO_2 molecules, which have a broad range of vibrational energies, give rise to CO products with a broad distribution of internal energies.

O(^{1}D) photofragments produced by channel (II) were detected at 205.47 nm (48 669 cm^{-1}) by using 2+1 REMPI via the ^{1}P$_1 \leftarrow {}^1$D$_2$ 2-photon transition. The c.m. KER distribution obtained by monitoring O(^{1}D) photofragments with high CO_2 heating is shown in Fig. 6.

The observed KER distribution peaks at ~300–400 cm^{-1} and extends to nearly 6000 cm^{-1}. As discussed above, with 230.1 nm photolysis the available energy must exceed 16 000 cm^{-1} in order to reach the threshold of channel (II). This is evident in the KER distributions of CO v″ = 0 (Fig. 3) where a new feature appears at 0–2000 cm^{-1}. With 205.47 nm (48 669 cm^{-1}) photolysis, CO_2 requires only ~11 000 cm^{-1} of internal energy to reach the threshold of Channel (II).

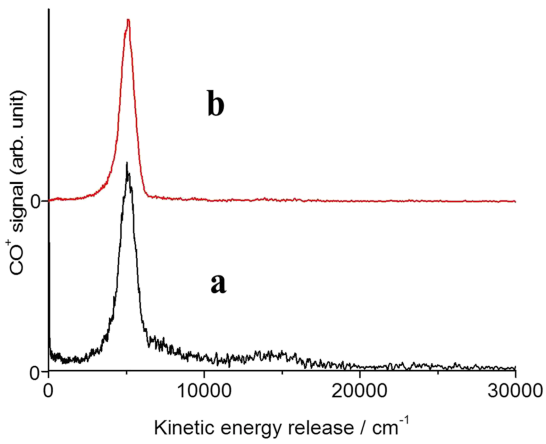

FIG. 4. c.m. KER distributions obtained with high CO_2 heating by monitoring (a) the bandhead of the $B \leftarrow X$ 1–1 transition at 230.27 nm, and (b) the peak of the M band at 230.34 nm. Signal intensities are normalized with respect to the feature centered at 5000 cm^{-1}.

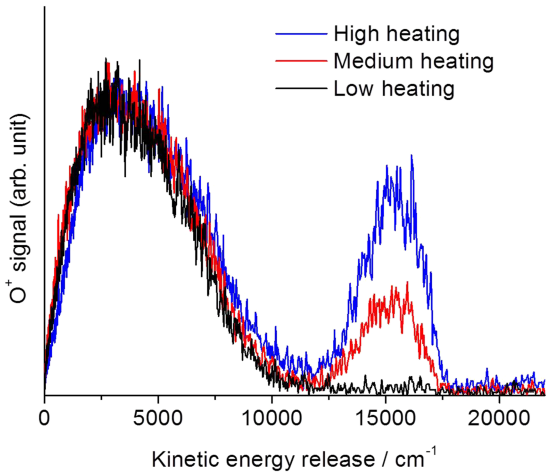

FIG. 5. c.m. KER distributions obtained by monitoring O(^{3}P$_2$) products at 225.654 nm with low (black), medium (red), and high (blue) CO_2 heating. The intensities of the KER distributions obtained with different heating levels are normalized with respect to the broad feature centered at ~3000 cm^{-1}.

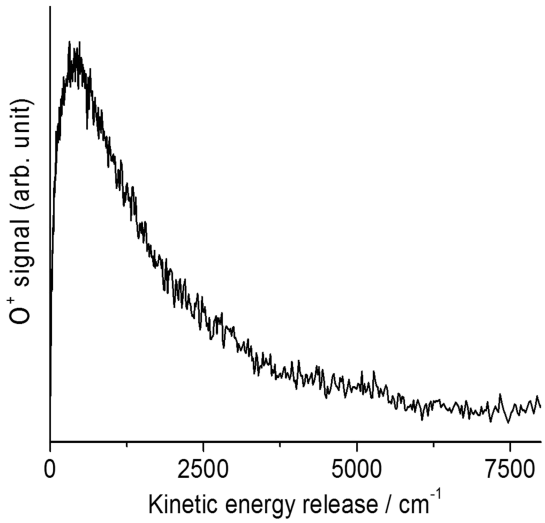

FIG. 6. c.m. KER distribution obtained by monitoring O(^{1}D) product at 205.47 nm with high CO_2 heating.

Hence, the c.m. KER of O(^{1}D) photofragments can extend up to 6000–7000 cm^{-1} when the internal energy of CO_2 is 17 000–18 000 cm^{-1}, as seen in Fig. 6. Clearly, the peak in the KER distribution is shifted to lower energies than the allowed maximum, indicating that the CO cofragments possess significant rovibrational excitation. We note again that parent CO_2 molecules with different rovibrational levels have different absorption cross sections and might also exhibit different photodissociation dynamics. All of these determine the final shape and maximum in the KER distribution obtained by monitoring O(^{1}D).

D. Implications to CO_2 photodissociation dynamics

As discussed in the Introduction, the absorption cross section of CO_2 at $\lambda > 190$ nm increases sharply with temperature, and absorption can extend up to 300 nm. Our study, which examines the 205–230 nm photodissociation of CO_2 at temperatures up to ~1800 K, extends the photodissociation studies of CO_2 to more realistic environments where thermally excited CO_2 is dissociated at much longer wavelengths than cold CO_2. It shows that several mechanisms are likely involved in dissociation via channels (I) and (II). The KER distributions shown in Fig. 3, which are obtained at different CO_2 temperatures, give an idea of the extent of vibrational excitation from which dissociation occurs at ~230 nm.

The REMPI spectra and KER distributions show that CO products are born with significant rovibrational excitation. A broad rovibrational state distribution in CO was observed also in the 157 nm photodissociation of cold CO_2, which is near the FC maximum of absorption to the $^1B_2$ state. At 157 nm, channel (II) was dominant,[21] but a minor channel (I) (about 6%) was also detected.[12,26,27] Understanding the dissociation dynamics is not easy even with supersonically cooled samples because the CO product state distributions span a broad energy range and the rotational populations exhibit fluctuations.[21] Our work demonstrates the increased complexity of the dissociation dynamics at higher temperatures and suggests that bending and stretch excitations of ground state CO_2 have a profound effect on the dissociation efficiency and dynamics.

Several theoretical studies have focused on the excited electronic states of CO_2 at 4–9 eV,[9–11,44,47,48] and on the interactions among states that are involved in the dissociation.[9,44] Schmidt *et al.* computed 1D potential energy curves for the electronic states of CO_2 as a function of OC–O internuclear distance (C_s) and OCO bond angle (C_{2v}).[9] Data on the five lowest singlet and triplet states that can be accessed below 8.5 eV (~68 500 cm^{-1}) are summarized in Table I, which lists both the vertical and adiabatic excitation energies. Figure 7 presents the corresponding schematic energy level diagram illustrating these states.

The calculated absorption spectrum at long wavelengths matches the experimental observations, and the photodissociation dynamics to channels (I) and (II) at 157 nm are also reproduced satisfactorily in the calculations.[9] It is concluded that whereas absorption is mainly to the A^1B_2 state at the vertical maximum, at longer wavelengths the B^1A_2 state can be excited as well (see below), and the long wavelength spectrum reflects also mixing between the A^1B_2 and the ground states.[9]

As listed in Table I, the energy differences between the ground and excited states decrease with decreasing OCO bond angle, e.g., with increased bending excitation in the ground electronic state. Our experiments show that heating CO_2 in the SiC tube imparts significant vibrational excitation that survives supersonic expansion. Due to more favorable FC factors, these internally hot CO_2 molecules absorb 205–230 nm radiation much more efficiently, allowing us to study the dissociation of CO_2 closer to the origins of the lowest excited states and to the dissociation threshold, where channel (I) dominates.

We emphasize that although the fraction of highly excited vibrational states is low (at 1800 K, the population of molecules with 20 000 cm^{-1} energy is only ~10^{-4} relative to the maximum), the steep increase in the absorption cross section with increasing vibrational excitation allows us to observe

TABLE I. Ground and excited electronic states of CO_2 taken from Ref. 9. Vertical and adiabatic excitation energies (V_{vert} and V_{min}, respectively) are listed. The geometries at the minimum of the potentials are given by the O–CO distance r_{min} and bond angle α_{min}.

Abbreviation	$D_{\infty h}$	C_{2v}	C_s	V_{vert} (eV)	V_{min} (eV)	r_{min}/a_0	α_{min} (deg)
X	$^1\Sigma_g^+$	1^1A_1	$1^1A'$	0	0	2.197	180
a	$^3\Sigma_u^+$	1^3B_2	$1^3A'$	8.228	4.642	2.355	117.5
b	$^3\Delta_u$	1^3A_2	$1^3A''$	8.713	5.329	2.370	127.4
B	$^1\Delta_u$	1^1A_2	$1^1A''$	8.950	5.528	2.370	127.2
A	$^1\Delta_u$	1^1B_2	$2^1A'$	8.938	5.532	2.363	117.8

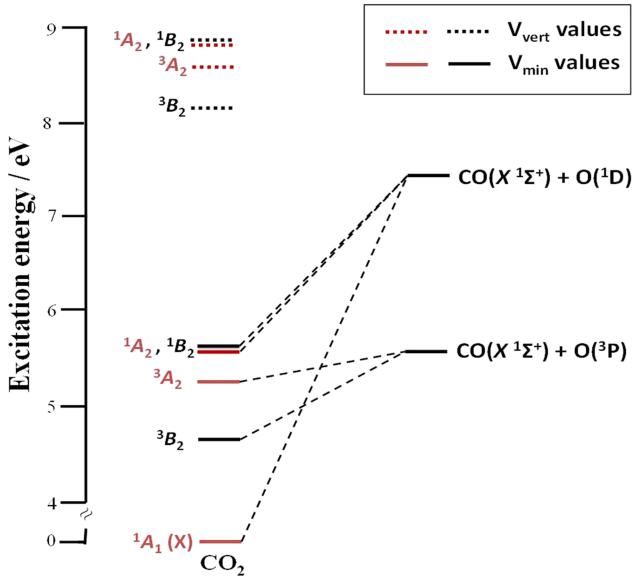

FIG. 7. Energy diagram showing adiabatic (V_{min}, solid line) and vertical (V_{vert}, dashed line) energies of the excited electronic states of CO_2 listed in Table I. *A* and *B* states are shown in red and black, respectively.

dissociation from these levels. As discussed in Section II, the vibrational population cannot be described by temperature due to the supersonic expansion. However, Fig. 3 shows that, as expected, the CO_2 vibrational levels appear in clumps, in accordance with the vibrational spectrum of CO_2 that displays a polyad structure even at high temperatures.[55]

Notably, the images recorded in our experiments are nearly isotropic ($\beta \sim 0$). A common reason for an isotropic product angular distribution is a dissociation lifetime that is longer than the rotational period of the molecule. In our case, the dissociation lifetime is unknown, and the average classical rotational period of CO_2 molecules at 100 K is roughly 0.9 ps. This may cause a decrease from the maximum recoil anisotropy value of 2.0 for a parallel transition. Previous studies of cold CO_2 photodissociation at 157 nm (63 690 cm^{-1}) showed that the fragments' angular distributions associated with channel (I) are anisotropic ($\beta = 1.25$), as expected for fast dissociation involving initial excitation via a parallel transition to the $^1B_2$ state.[17,85] In contrast, the angular distributions of CO fragments produced via channel (II) at the same wavelength are nearly isotropic,[21] with β decreasing strongly with decreasing kinetic energy and CO rovibrational excitation, even though the initially excited state is short lived.[17] It was proposed that the initially excited state may have crossed to a predissociative state whose lifetime is longer than the rotational period of CO_2.[21] Another plausible argument put forward is that dissociation occurs from bent vibrational configurations or high rotational levels that reduce the anisotropy by changing the fragments' recoil direction. In our experiments, CO_2 molecules with even higher vibrational excitation are electronically excited. If dissociation takes place from vibrational configurations with high bending excitation, the anisotropy would be reduced.

Another likely reason for the reduced anisotropy is the concurrent excitation to the $^1B_2$ and $^1A_2$ states, which are reached via parallel and perpendicular transitions, respectively. Schmidt and coworkers showed that at long wavelengths there are reasonable transition dipole moments (TDMs) to both of these states, and the bending and asymmetric stretch excitations increase the TDM to $^1A_2$.[9] Spielfiedel *et al.* assigned a long bending progression of perpendicular bands to transitions to the B^1A_2 state at the long wavelength absorption tail, in addition to the main bands to the A^1B_2 excited state.[8] The nearly isotropic KER distributions of the products measured in our experiments suggest that both these excited states participate in the initial electronic excitation, and this may be a major cause for the reduction in anisotropy.

The main photodissociation products observed in our studies derive from the spin-forbidden channel (I). With 157 nm photodissociation of CO_2, this was the minor channel, accounting for merely a few percent relative to channel (II).[12,21] Evidently in dissociation via channel (I), spin-orbit coupling must be involved, and therefore the reverse spin-forbidden recombination reaction, O(^{3}P) + CO, is also relevant to our work. It has been established long ago that the so-called "CO flame bands," which derive from the recombination of O(^{3}P) and CO, result in weak emission from the $^1B_2$ excited state of CO_2.[86] Several recent theoretical papers have examined the recombination reaction, identifying spin-orbit couplings and conical intersections.[11,44–48] Even though these calculations do not include the highly excited CO_2 vibrational levels that are necessary to describe fully our results, they indicate that more than one reaction mechanism must be involved. The calculations show the participation of a direct (or non-statistical) mechanism, which is too fast to allow for randomization of energy, and an indirect (or statistical-like) route, in which at least some energy randomization takes place. The exact nature of the dynamics via these two pathways is not settled yet, but the outcome is clear. Jasper and Dawes, for example, find that both the a^3B_2 and b^3A_2 triplet states are involved in the spin-forbidden reaction O(^{1}D) + CO → CO + O(^{3}P).[47] In addition, the authors highlight the importance of including geometry dependence in the spin-orbit coupling surface. In considering the coupling between the electronic ground state and the lowest triplet a^3B_2 state, Jasper and Dawes[47] and Hwang and Mebel[44] conclude that both direct and indirect mechanisms are involved. Jasper and Dawes suggest that the relative importance of these two mechanisms depends on the depth of the geometry-dependent entrance channel well, in addition to the properties of the saddle point and the energy minimum in the spin-orbit crossing seam. In our studies, a broad range of geometries is sampled, which is likely to affect the dynamics to an even greater extent. The existence of multiple dynamical channels is amply evidenced in the KER distributions of the CO and O products, and also in the CO REMPI spectra obtained as a function of CO_2 heating. In dissociation events that start closer to the reaction threshold, as is the case in our work, it is not hard to imagine that following initial excitation to either the A^1B_2 or B^1A_2 state or both, the a^3B_2 and b^3A_2 triplet states and even the ground electronic state are involved, giving rise to multiple crossings and dissociation pathways that depend sensitively on initial vibrational excitation of parent CO_2.

IV. SUMMARY AND CONCLUSIONS

The 205–230 nm photodissociation of vibrationally excited CO_2 at temperatures up to 1800 K was studied in a molecular beam by using REMPI spectroscopy and time-sliced VMI. Upon heating, dissociation from vibrational levels with energy up to nearly 20 000 cm^{-1} was detected, giving rise to CO, $O(^3P)$, and $O(^1D)$ products (channel (I) and (II)). The large enhancement of the absorption cross section with increasing CO_2 vibrational excitation made the investigation of photodissociation from highly vibrationally excited molecules feasible. It is likely that initial absorption is to both the A^1B_2 and B^1A_2 states.

We show that CO_2 must have a minimum internal energy of ~4000 cm^{-1} in order to absorb 230 nm radiation, in good agreement with previous estimates.[40,42,43] 2+1 REMPI spectra of the CO products show that $v'' = 0$ and 1 are generated in a broad range of rotational states, but direct REMPI identification of higher vibrational levels was hampered by uncertainties in the spectroscopic assignment. Nevertheless, fits of the rotational distributions of CO $v'' = 0$ show that at higher CO_2 temperatures the rotational distributions are bimodal; they can be fit with a ~1700 K Boltzmann component at low to medium J'' levels, and a narrow Gaussian-shaped component centered at $J'' > 40$.

The fragments KER distributions obtained by monitoring the CO $B \rightarrow X$ (0–0) bandhead reveal the extent of vibrational excitation in the parent CO_2, which increases with heating. Direct detection of hot CO_2, albeit with less sensitivity, was achieved by 3+1 REMPI as described in the supplementary material (Fig. S6 and Table S7). State specific dynamics in the photodissociation of hot CO_2 is suggested, among others, by the KER distributions observed when monitoring the M REMPI band (Fig. 4(b)), which show only a narrow range of KER distributions centered at ~5000 cm^{-1}. However, the dynamics responsible for this state-specific KER distribution remain unexplained, as is the exact assignment of the M band (Fig. 1).

The extent of rovibrational excitation in the CO product is assessed from KER distributions obtained by monitoring the $O(^3P)$ and $O(^1D)$ fragments. All spin-orbit states of $O(^3P)$ are produced in the dissociation and have similar KER distributions. With low CO_2 heating, the KER distribution obtained by monitoring $O(^3P)$ is broad and unstructured, corresponding to highly rovibrationally excited CO cofragments. At higher temperatures, a second unstructured component centered at high KER appears, indicating the opening of another, more direct, dissociation pathway. Following 205 nm dissociation, the KER distributions obtained by monitoring the $O(^1D)$ fragment, which have 16 000 cm^{-1} of internal energy, peak at lower KER values but extend up to about 6000 cm^{-1}. These distributions show that CO fragments associated with channel (II) are also born with a broad distribution of rovibrational levels.

While detailed theoretical descriptions of the dissociation dynamics are unavailable at this time (and maybe unfeasible), the observation that several dynamical pathways contribute to the observed fragments' REMPI spectra and KER distributions is hardly surprising. Theoretical calculations of the absorption spectrum of CO_2, especially in the long wavelength tail, show that optical excitation can reach both the A^1B_2 or B^1A_2 excited singlet states, and that vibrational excitation can strongly enhance absorption and change the relative contributions of these two absorption systems. Electronic structure calculations of the conical intersections among states of the same multiplicity and spin-orbit couplings between states of different multiplicities, which are still incomplete, show that the low-lying excited electronic states can interact either directly or via the ground electronic state, and that both the a^3B_2 and b^3A_2 triplet states are likely involved in dissociation via channel (I). Theory shows that reaction pathways can be direct, without energy randomization in the shallow wells in the excited states, or more statistical-like involving partial or total randomization of energy in the excited states during conical intersection or in reaching the spin-orbit crossing seams.

Because the photodissociation involves intermediate states with shallow wells, it is expected that state-specific effects with respect to initial vibrational excitation of the parent CO_2 molecule would be important. A more detailed view of the dissociation mechanism may be obtained by exploiting vibrationally mediated photodissociation to reach specific vibrational levels of CO_2 directly and explore their photodissociation. Excitation of combination bands with stretch and bend components should be particularly fruitful.

SUPPLEMENTARY MATERIAL

See supplementary material for 2+1 REMPI spectroscopy of CO and $O(^3P)$, 3+1 REMPI spectroscopy of hot CO_2, and KER distributions obtained by monitoring $CO(v'' = 0)$ at higher J''s.

ACKNOWLEDGMENTS

Support by the U.S. Department of Energy, Basic Energy Sciences, Grant No. DE-FG02-05ER15629, is gratefully acknowledged.

[1] J. Jeffries, C. Schulz, D. Mattison, M. Oehlschlaeger, W. Bessler, T. Lee, D. Davidson, and R. Hanson, Proc. Combust. Inst. **30**, 1591 (2005).
[2] C. Schulz, J. Jeffries, D. Davidson, J. Koch, J. Wolfrum, and R. Hanson, Proc. Combust. Inst. **29**, 2735 (2002).
[3] T. Settersten, A. Dreizler, B. Patterson, P. Schrader, and R. Farrow, Appl. Phys. B **76**, 479 (2003).
[4] A. Anbar, M. Allen, and H. Nair, J. Geophys. Res.: Planets **98**, 10925, doi:10.1029/93je00330 (1993).
[5] M. B. McElroy, N. Dak Sze, and Y. Ling Yung, J. Atmos. Sci. **30**, 1437 (1973).
[6] O. Venot, N. Fray, Y. Bénilan, M.-C. Gazeau, E. Hébrard, G. Larcher, M. Schwell, M. Dobrijevic, and F. Selsis, Astron. Astrophys. **551**, A131 (2013).
[7] Y. L. Yung and W. B. DeMore, *Photochemistry of Planetary Atmospheres* (Oxford University Press, 1999).
[8] A. Spielfiedel, N. Feautrier, C. Cossart-Magos, G. Chambaud, P. Rosmus, H. J. Werner, and P. Botschwina, J. Chem. Phys. **97**, 8382 (1992).
[9] J. A. Schmidt, M. S. Johnson, and R. Schinke, Proc. Natl. Acad. Sci. U. S. A **110**, 17691 (2013).
[10] S. Y. Grebenshchikov, J. Chem. Phys. **138**, 224107 (2013).
[11] B. Zhou, C. Zhu, Z. Wen, Z. Jiang, J. Yu, Y.-P. Lee, and S. H. Lin, J. Chem. Phys. **139**, 154302 (2013).
[12] Z. Chen, F. Liu, B. Jiang, X. Yang, and D. H. Parker, J. Phys. Chem. Lett. **1**, 1861 (2010).
[13] H. Gao, Y. Song, W. M. Jackson, and C. Ng, J. Chem. Phys. **138**, 191102 (2013).

[14]H. Gao, Y. Song, L. Yang, X. Shi, Q.-Z. Yin, C. Ng, and W. M. Jackson, J. Chem. Phys. **137**, 034305 (2012).
[15]M. Koshi, M. Yoshimura, and H. Matsui, Chem. Phys. Lett. **176**, 519 (1991).
[16]I. Koyano, T. Wauchop, and K. Welge, J. Chem. Phys. **63**, 110 (1975).
[17]I.-C. Lu, J. J. Lin, S.-H. Lee, Y. T. Lee, and X. Yang, Chem. Phys. Lett. **382**, 665 (2003).
[18]Z. Lu, Y. C. Chang, Y. Benitez, Z. Luo, A. B. Houria, T. Ayari, M. M. Al Mogren, M. Hochlaf, W. Jackson, and C. Ng, Phys. Chem. Chem. Phys. **17**, 11752 (2015).
[19]Z. Lu, Y. C. Chang, H. Gao, Y. Benitez, Y. Song, C. Ng, and W. Jackson, J. Chem. Phys. **140**, 231101 (2014).
[20]Z. Lu, Y. C. Chang, Q.-Z. Yin, C. Ng, and W. M. Jackson, Science **346**, 61 (2014).
[21]R. Miller, S. Kable, P. Houston, and I. Burak, J. Chem. Phys. **96**, 332 (1992).
[22]Y. Pan, H. Gao, L. Yang, J. Zhou, C. Ng, and W. M. Jackson, J. Chem. Phys. **135**, 071101 (2011).
[23]T. Slanger, R. Sharpless, and G. Black, J. Chem. Phys. **67**, 5317 (1977).
[24]Y. Song, H. Gao, Y. C. Chang, Z. Lu, C. Ng, and W. M. Jackson, Phys. Chem. Chem. Phys. **16**, 563 (2014).
[25]A. Stolow and Y. T. Lee, J. Chem. Phys. **98**, 2066 (1993).
[26]Y. F. Zhu and R. J. Gordon, J. Chem. Phys. **92**, 2897 (1990).
[27]Y. Matsumi, N. Shafer, K. Tonokura, M. Kawasaki, Y. L. Huang, and R. J. Gordon, J. Chem. Phys. **95**, 7311 (1991).
[28]S. P. McGlynn, J. W. Rabalais, J. R. McDonald, and V. Scherr, Chem. Rev. **71**, 73 (1971).
[29]H. L. Berghout, F. F. Crim, M. Zyrianov, and H. Reisler, J. Chem. Phys. **112**, 6678 (2000).
[30]T. Droz-Georget, M. Zyrianov, H. Reisler, and D. W. Chandler, Chem. Phys. Lett. **276**, 316 (1997).
[31]T. Droz-Georget, M. Zyrianov, A. Sanov, and H. Reisler, Ber. Bunsenges. Phys. Chem. **101**, 469 (1997).
[32]M. Zyrianov, T. Droz-Georget, and H. Reisler, J. Chem. Phys. **110**, 2059 (1999).
[33]M. Zyrianov, T. Droz-Georget, A. Sanov, and H. Reisler, J. Chem. Phys. **105**, 8111 (1996).
[34]S. S. Brown, H. L. Berghout, and F. F. Crim, J. Chem. Phys. **102**, 8440 (1995).
[35]S. S. Brown, R. B. Metz, H. L. Berghout, and F. F. Crim, J. Chem. Phys. **105**, 6293 (1996).
[36]W. Parkinson, J. Rufus, and K. Yoshino, Chem. Phys. **290**, 251 (2003).
[37]K. Yoshino, J. Esmond, Y. Sun, W. Parkinson, K. Ito, and T. Matsui, J. Quant. Spectrosc. Radiat. Transfer **55**, 53 (1996).
[38]R. J. Jensen, R. D. Guettler, and J. L. Lyman, Chem. Phys. Lett. **277**, 356 (1997).
[39]M. A. Oehlschlaeger, D. F. Davidson, and J. B. Jeffries, Appl. Opt. **44**, 6599 (2005).
[40]M. A. Oehlschlaeger, D. F. Davidson, J. B. Jeffries, and R. K. Hanson, Chem. Phys. Lett. **399**, 490 (2004).
[41]C. Schulz, J. Koch, D. Davidson, J. Jeffries, and R. Hanson, Chem. Phys. Lett. **355**, 82 (2002).
[42]L. Ibraguimova, B. Minaev, and I. Irgibaeva, Opt. Spectrosc. **117**, 695 (2014).
[43]T. Lee, W. Bessler, J. Yoo, C. Schulz, J. Jeffries, and R. Hanson, Appl. Phys. B **93**, 677 (2008).
[44]D.-Y. Hwang and A. M. Mebel, Chem. Phys. **256**, 169 (2000).
[45]L. Ibraguimova and B. Minaev, Opt. Spectrosc. **120**, 345 (2016).
[46]A. W. Jasper, J. Phys. Chem. A **119**, 7339 (2015).
[47]A. W. Jasper and R. Dawes, J. Chem. Phys. **139**, 154313 (2013).
[48]Y. Ma, L. Peng, H. Zhang, and J.-G. Yu, Russ. J. Phys. Chem. A **88**, 2339 (2014).
[49]E. Fermi, Z. Phys. **71**, 250 (1931).
[50]C. E. Miller and L. R. Brown, J. Mol. Spectrosc. **228**, 329 (2004).
[51]L. Régalia-Jarlot, V. Zéninari, B. Parvitte, A. Grossel, X. Thomas, P. Von der Heyden, and G. Durry, J. Quant. Spectrosc. Radiat. Transfer **101**, 325 (2006).
[52]L. Rothman, I. Gordon, R. Barber, H. Dothe, R. Gamache, A. Goldman, V. Perevalov, S. Tashkun, and J. Tennyson, J. Quant. Spectrosc. Radiat. Transfer **111**, 2139 (2010).
[53]L. Rothman, R. Hawkins, R. Wattson, and R. Gamache, J. Quant. Spectrosc. Radiat. Transfer **48**, 537 (1992).
[54]K.-F. Song, Y. Lu, Y. Tan, B. Gao, A.-W. Liu, and S.-M. Hu, J. Quant. Spectrosc. Radiat. Transfer **112**, 761 (2011).
[55]S. A. Tashkun, V. I. Perevalov, J.-L. Teffo, A. D. Bykov, and N. Lavrentieva, J. Quant. Spectrosc. Radiat. Transfer **82**, 165 (2003).
[56]R. Toth, L. Brown, C. Miller, V. M. Devi, and D. C. Benner, J. Quant. Spectrosc. Radiat. Transfer **109**, 906 (2008).
[57]H. W. Rohrs, C. T. Wickham-Jones, G. B. Ellison, D. Berry, and B. M. Argrow, Rev. Sci. Instrum. **66**, 2430 (1995).
[58]Q. Guan, K. N. Urness, T. K. Ormond, D. E. David, G. B. Ellison, and J. W. Daily, Int. Rev. Phys. Chem. **33**, 447 (2014).
[59]D. W. Kohn, H. Clauberg, and P. Chen, Rev. Sci. Instrum. **63**, 4003 (1992).
[60]G. S. Wyszecki and W. Stiles, *Color Science: Concepts and Methods, Quantitative Data and Formulae* (John Wiley & Sons, New York, 1982).
[61]B. Fortner and T. E. Meyer, *Number by Colors: A Guide to Using Color to Understand Technical Data* (Springer Science & Business Media, 2012).
[62]X. Zhang, A. V. Friderichsen, S. Nandi, G. B. Ellison, D. E. David, J. T. McKinnon, T. G. Lindeman, D. C. Dayton, and M. R. Nimlos, Rev. Sci. Instrum. **74**, 3077 (2003).
[63]P. J. Tjossem and K. C. Smyth, J. Chem. Phys. **91**, 2041 (1989).
[64]D. J. Bamford, M. J. Dyer, and W. K. Bischel, Phys. Rev. A **36**, 3497 (1987).
[65]S. T. Pratt, P. M. Dehmer, and J. L. Dehmer, Phys. Rev. A **43**, 282 (1991).
[66]M. Wu and P. M. Johnson, J. Chem. Phys. **91**, 7399 (1989).
[67]C. P. Rodrigo, S. Sutradhar, and H. Reisler, J. Phys. Chem. A **118**, 11916 (2014).
[68]M. Ryazanov and H. Reisler, J. Chem. Phys. **138**, 144201 (2013).
[69]M. Ryazanov, C. Rodrigo, and H. Reisler, J. Chem. Phys. **136**, 084305 (2012).
[70]M. Eidelsberg, J.-Y. Roncin, A. Le Floch, F. Launay, C. Letzelter, and J. Rostas, J. Mol. Spectrosc. **121**, 309 (1987).
[71]A. M. Rijs, E. H. Backus, C. A. de Lange, M. H. Janssen, N. P. Westwood, K. Wang, and V. McKoy, J. Chem. Phys. **116**, 2776 (2002).
[72]C. Western, PGOPHER, edition 7, a program for simulating rotational structure, 2010.
[73]J. M. Seitzman, J. Haumann, and R. K. Hanson, Appl. Opt. **26**, 2892 (1987).
[74]T. A. Spiglanin, R. A. Perry, and D. W. Chandler, J. Chem. Phys. **87**, 1568 (1987).
[75]J. Baker, Chem. Phys. Lett. **408**, 312 (2005).
[76]S. Federman, M. Fritts, S. Cheng, K. Menningen, D. C. Knauth, and K. Fulk, Astrophys. J., Suppl. Ser. **134**, 133 (2001).
[77]C. Letzelter, M. Eidelsberg, F. Rostas, J. Breton, and B. Thieblemont, Chem. Phys. **114**, 273 (1987).
[78]J. Baker, W. Ü. L. Tchang-Brillet, and P. S. Julienne, J. Chem. Phys. **102**, 3956 (1995).
[79]M. Eidelsberg, F. Launay, K. Ito, T. Matsui, P. C. Hinnen, E. Reinhold, W. Ubachs, and K. P. Huber, J. Chem. Phys. **121**, 292 (2004).
[80]W. Ü. L. Tchang-Brillet, P. Julienne, J. M. Robbe, C. Letzelter, and F. Rostas, J. Chem. Phys. **96**, 6735 (1992).
[81]N. Mina-Camilde, C. Manzanares, and J. F. Caballero, J. Chem. Educ. **73**, 804 (1996).
[82]J. Baker and F. Launay, J. Mol. Spectrosc. **165**, 75 (1994).
[83]G. Berden, R. T. Jongma, and G. Meijer, J. Chem. Phys. **107**, 8303 (1997).
[84]M. Eidelsberg and F. Rostas, Astron. Astrophys. **235**, 472 (1990).
[85]P. Chen, C. Ng, T. Baer, and I. Powis, *Unimolecular and Bimolecular Reaction Dynamics* (John Wiley & Sons, New York, 1994).
[86]R. Dixon, in *Proceedings of the Royal Society of London A: Mathematical, Physical and Engineering Sciences* (The Royal Society, 1963), p. 431.